Macromolecules

Article

pubs.acs.org/Macromolecules

Emergence and Stability of Helical Superstructures in ABC Triblock Copolymers

Weihua Li* and Feng Qiu*

State Key Laboratory of Molecular Engineering of Polymers, Department of Macromolecular Science, Fudan University, Shanghai 200433, China

An-Chang Shi*

Department of Physics and Astronomy, McMaster University, Hamilton, Ontario, Canada, L8S 4M1

ABSTRACT: The emergence and stability of superstructured cylindrical phases in frustrated ABC linear triblock copolymers are investigated by the self-consistent field theory. Our results reveal that the complex single/double/triple helices-on-cylinder phases are formed when the straight cylinders-on-cylinder and rings-on-cylinder phases are frustrated due to packing constraints. A free energy comparison indicates that the double and triple helical phases are stable, whereas the other cylinders-on-cylinder phases are metastable. In addition, the chirality and rotation for the helical supercylinders are considered in our calculations. Our theoretical prediction is consistent with a number of experimental observations.

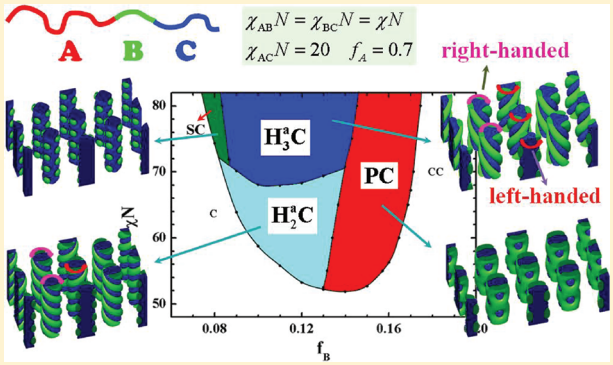

I. INTRODUCTION

The formation of helical structures is a fascinating yet generic behavior in nature. Besides the most well-known examples of α-helices in proteins and DNA double-strand helices, helices also arise in screws, springs, tendrils, vines, and so on.[1] The propensity of helices in nature has attracted tremendous attention to the origin of helical structures. Motivated by nature, polymer scientists have been searching for and studying helical structures formed from the self-assembly of synthetic polymers. Similar to the α-helices in proteins, chiral centers can be introduced into synthetic polymers. It has been shown that diblock copolymer composed of at least one chiral block can self-assemble into helical structures.[2−4] What is more fascinating is that helical structures can also spontaneously form in cylinder-forming achiral diblock copolymers confined in a cylindrical nanopore,[5−12] and in softly confined achiral ABC star[13] and linear triblock copolymers (or solution systems).[14] In addition, helical structures have also been observed in melts of complex block copolymers such as ABC linear triblock copolymers. Understanding the formation and stability of these helical superstructures from achiral block copolymers in bulk presents an interesting challenge in soft matter theory.

In the present paper we focus on the formation and stability of helical superstructures from linear ABC triblock copolymer melts. Because of the large number of controlling parameters and topological constraints, ABC triblock copolymers exhibit an extreme rich phase behavior.[15] Their sophisticated self-assembling capabilities have made ABC triblock copolymers an important platform for the engineering of new ordered phases, which may have potential applications for fabrication techniques of functional materials.[16,17] According to the relative strength of the three Flory−Huggins interaction parameters, χ_{AB}, χ_{BC}, and χ_{AC}, the phase behavior of triblock copolymer melts can be classified into "nonfrustrated" and "frustrated" cases.[18] In the nonfrustrated case, the repulsion between the two end-blocks, χ_{AC}, is comparable to or larger than the repulsion between the neighboring blocks, χ_{AB} and χ_{BC}, thus the A and C blocks prefer to be separated, forming distinct A/B and B/C interfaces. This type of structures do not frustrate the topology of the linear ABC chain architecture. In the frustrated case, the repulsion between the two end-blocks, χ_{AC}, is weaker than the repulsions between the neighboring blocks, χ_{AB} or χ_{BC}, thus the block copolymers prefer structures with larger A/C interfaces. However the formation of A/C interfaces is not commensurate with the topology of the linear ABC triblock copolymers, resulting in the formation of complex ordered phases to alleviate the topological frustration. The phase behaviors of triblock copolymers have been extensively studied by experiments and theories.[19]

Because of the simplicity of the core−shell or alternated structures, theoretical framework based on the spectral method for the study of the phase behavior of nonfrustrated ABC triblock copolymers has been well developed.[20−22] On the

Received: October 27, 2011
Revised: November 26, 2011
Published: December 12, 2011

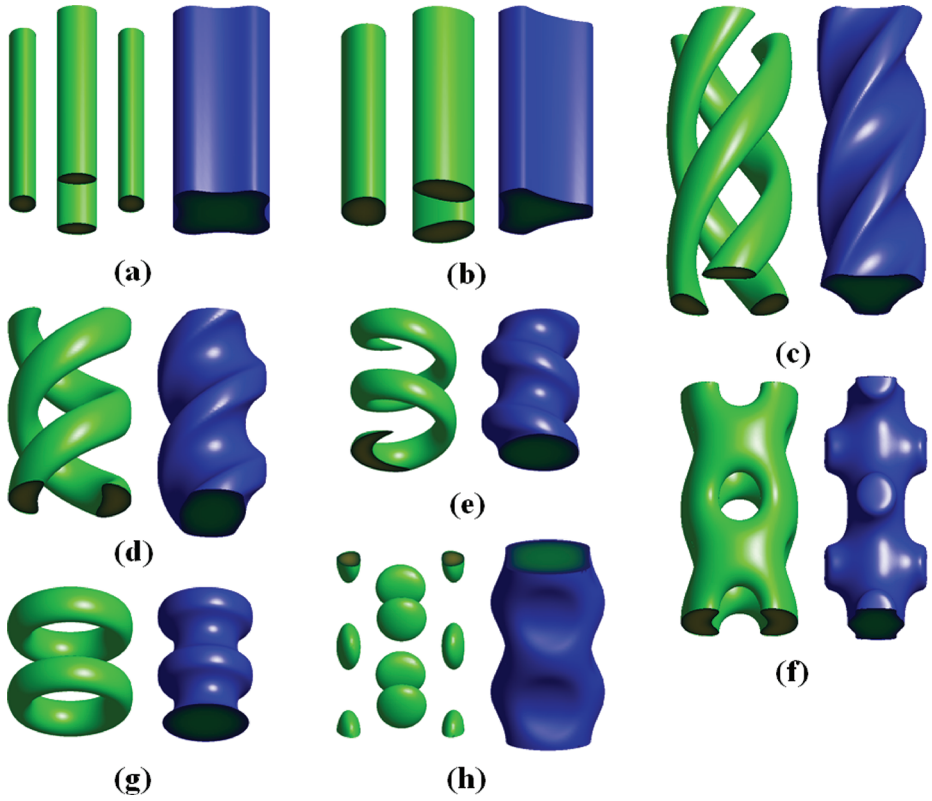

Figure 1. Isosurfaces for ϕ_B (green) and ϕ_C (blue) of superstructures formed in frustrated ABC linear triblock copolymers: (a) quadruple cylinders-on-cylinder (C_4C); (b) triple cylinders-on-cylinder (C_3C); (c) triple helices-on-cylinder (H_3C); (d) double helices-on-cylinder (H_2C); (e) single helix-on-cylinder (C_3C); (f) perforated-lamella-on-cylinder (PC); (g) rings-on-cylinder (RC); (h) spheres-on-cylinder (SC).

other hand, the ordered phases formed from frustrated triblock copolymers change from the core−shell type or alternating type to superstructured or hierarchical structures, such as cylinders-on-lamellae, spheres-on-lamellae, cylinders-on-cylinder, spheres-on-cylinder, and so on. Theoretical investigation of these complex structures has been carried out by a generic spectral method of the self-consistent field theory (SCFT).[23] The generic spectral method is an efficient tool for the search of possible ordered phases. However, the determination of precise phase diagrams using the spectral method requires a large number of basis functions. In the current study, we apply the pseudospectral method,[24−26] coupled with the knowledge of the symmetry of the ordered phases, to examine the formation and stability of complex ordered phases of frustrated triblock copolymers. We will focus on one type of complex ordered phases, i.e., hierarchical phases of hexagonal cylinders, where the large cylinders are decorated by various substructures. A number of supercylindrical phases, including cylinders-on-cylinder and spheres-on-cylinder, have been either observed or postulated in previous experiments or theories.[15,19,27−36] The cylinders-on-cylinder phases are of great interest because the substructures of cylinders can be straight cylinders, or helices, or rings. In addition, for the cases of straight cylinders and helices, the cylinder/helix number is another quantity to vary the supercylindrical phase. For example, the helical number of the helical supercylinders, formed in the poly(styrene-*b*-butadiene-*b*-methyl methacrylate) (PS−PB-PMMA) triblock copolymers, was proposed to be four,[29] and recently it was determined to be two by 3D transmission electron microtomography (TEMT).[34] To date, there is no direct proof to support that there is no other helical phase except for the double-helical one, such as single-helical, triple-helical, or four-helical phase. Furthermore, the relative stability of these helical phases to those straight cylinders-on-cylinder phases is unknown. Therefore, a theoretical study to explore the supercylindrical phase behaviors of frustrated ABC linear triblock copolymers is desirable. In this paper, we report a theoretical study of these complex superstructures within the framework of SCFT. Specifically, we use the pseudospectral method, coupled with special initial conditions, to compute the free energy of a number of candidate structures, thus determining the relative stability of these phases.

II. THEORY

We consider an incompressible melt of ABC linear triblock copolymers with a degree of polymerization N in a volume of V. The chain lengths of A, B and C blocks are specified by f_AN, f_BN, and f_CN ($f_A + f_B + f_C = 1$), respectively. The interactions between the three dissimilar monomers are characterized by three Flory−Huggins interaction parameters, χ_{AB}, χ_{AC}, and χ_{BC}. The radius of gyration of the polymer, R_g, is set as the unit of spatial lengths in our calculations. Within the mean-field approximation to statistical mechanics of the Edwards model of polymers,[26,37] the free energy functional F for n Gaussian triblock copolymer chains at a given temperature T is given by,

$$\frac{F}{nk_BT} = -\ln Q + \frac{1}{V}\int d\mathbf{r}\,\{\chi_{AB}N\phi_A(\mathbf{r})\phi_B(\mathbf{r}) + \chi_{AC}N\phi_A(\mathbf{r})\phi_C(\mathbf{r}) + \chi_{BC}N\phi_B(\mathbf{r})\phi_C(\mathbf{r}) - \omega_A(\mathbf{r})\phi_A(\mathbf{r}) - \omega_B(\mathbf{r})\phi_B(\mathbf{r}) - \omega_C(\mathbf{r})\phi_C(\mathbf{r}) - \eta(\mathbf{r})[1 - \phi_A(\mathbf{r}) - \phi_B(\mathbf{r}) - \phi_C(\mathbf{r})]\} \quad (1)$$

dx.doi.org/10.1021/ma2023952 | *Macromolecules* 2012, 45, 503−509

Here ϕ_A, ϕ_B, and ϕ_C are the monomer densities. The quantity Q is the partition function of a single polymer chain interacting with the mean fields ω_A, ω_B, and ω_C, which are produced by the surrounding chains. Minimization of the free energy with respect to the monomer densities and the mean fields leads to the following standard SCFT equations[26]

$$\omega_A(\mathbf{r}) = \chi_{AB}N\phi_B(\mathbf{r}) + \chi_{AC}N\phi_C(\mathbf{r}) + \eta(\mathbf{r})$$
$$\omega_B(\mathbf{r}) = \chi_{AB}N\phi_A(\mathbf{r}) + \chi_{BC}N\phi_C(\mathbf{r}) + \eta(\mathbf{r})$$
$$\omega_C(\mathbf{r}) = \chi_{AC}N\phi_A(\mathbf{r}) + \chi_{BC}N\phi_B(\mathbf{r}) + \eta(\mathbf{r})$$
$$\phi_A(\mathbf{r}) = \frac{1}{Q}\int_0^{f_A} \mathrm{d}s\, q(\mathbf{r}, s)q^{\dagger}(\mathbf{r}, s)$$
$$\phi_B(\mathbf{r}) = \frac{1}{Q}\int_{f_A}^{f_A+f_B} \mathrm{d}s\, q(\mathbf{r}, s)q^{\dagger}(\mathbf{r}, s)$$
$$\phi_C(\mathbf{r}) = \frac{1}{Q}\int_{1-f_C}^{1} \mathrm{d}s\, q(\mathbf{r}, s)q^{\dagger}(\mathbf{r}, s)$$
$$Q = \frac{1}{V}\int \mathrm{d}\mathbf{r}\, q(\mathbf{r}, s)q^{\dagger}(\mathbf{r}, s)$$
$$\phi_A(\mathbf{r}) + \phi_B(\mathbf{r}) + \phi_C(\mathbf{r}) = 1 \qquad (2)$$

In the above equations, $q(\mathbf{r},s)$ and $q^{\dagger}(\mathbf{r},s)$ are end-segment distribution functions.[26] These distribution functions satisfy the modified diffusion equations

$$\frac{\partial q(\mathbf{r}, s)}{\partial s} = \nabla^2 q(\mathbf{r}, s) - \omega(\mathbf{r}, s)q(\mathbf{r}, s) \qquad (3)$$

$$-\frac{\partial q^{\dagger}(\mathbf{r}, s)}{\partial s} = \nabla^2 q^{\dagger}(\mathbf{r}, s) - \omega(\mathbf{r}, s)q^{\dagger}(\mathbf{r}, s) \qquad (4)$$

where $\omega(\mathbf{r},s) = \omega_K(\mathbf{r})$ when s belongs to K blocks (K = A, B, C). The initial conditions are $q(\mathbf{r},0) = q^{\dagger}(\mathbf{r},1) = 1$. For numerical solutions, we employ the second-order operator-split method (or the pseudospectral method)[2425,] to solve the modified diffusion equations for the end-segment distribution functions.

III. RESULTS AND DISCUSSION

We assume that the A-block has the largest volume fraction thus the A-blocks form the matrix of the phases. The candidate ordered phases are formed by C-cylinders arranged in the A-matrix, where the A/C interfaces are decorated by B-substructures. Besides the simple cylinders (C) and B/C core−shell cylinders (CC), there are eight cylindrical superstructures examined in the current study (Figure 1): (a) quadruple straight cylinders-on-cylinder (C_4C), (b) triple straight cylinders-on-cylinder (C_3C), (c) triple helices-on-cylinder (H_3C), (d) double helices-on-cylinder (H_2C), (e) single helix-on-cylinder (H_1C), (f) perforated-lamella-on-cylinder (PC), (g) rings-on-cylinder (RC), and (h) spheres-on-cylinder (SC). These ordered phases are obtained from the SCFT calculations by using initial conditions bearing their symmetries. In practice, first we set the axial direction of cylinder along the z-direction, and the perpendicular cross-section to the xy-plane. Then the hexagonal symmetry is imposed on the arrangement of cylinders. We parallelize[38] the pseudospectral method to solve the modified diffusion equations for the end-segment distribution functions, using the fast-Fourier transform (FFTW) libraries.[39] Usually two unit cells for each structure are put into a cuboidal box which is discretized into a $N_x \times N_y \times N_z = 128 \times 128 \times 64$ lattice. We impose periodic boundary conditions on all edges of the cubic lattice. The free energy is minimized with respect to the size of the simulation box. The chain contour length for the copolymer is discretized with $\Delta s = 0.01$, and the trapezoidal scheme is used to carry out integration along s. During the iteration steps to solve the SCFT equations, a simple linear mixing scheme is used to update the fields for each iteration. The convergence is judged by ensuring the free energy and the incompressibility condition to an accuracy of about 10^{-7}.

As a typical example of frustrated triblock copolymers, we will use the parameter set such that $\chi_{AC}N \ll \chi_{AB}N = \chi_{BC}N = \chi N$. This assumption is reasonable for typical frustrated systems studied in experiments, such as poly(styrene-*b*-butadiene-*b*-methyl methacrylate) (PS−PB−PMMA),[28,29,31,34] poly(styrene-*b*-ethylene-*co*-butylene-*b*-methyl methacrylate)(PS−PEB−PMMA),[27,28] and poly(styrene-*b*-2-vinylpyridine-*b*-tert-butyl methacrylate) (PS−P2VP−PtBMA).[32,33] The phase behavior is presented by two typical phase diagrams. The first one is the portion of the supercylindrical phase region between $f_A = 0.68$ and $f_A = 0.76$ in the triangular phase diagram with $\chi N = 80$ and $\chi_{AC}N = 20$ (Figure 2). The choice of this composition

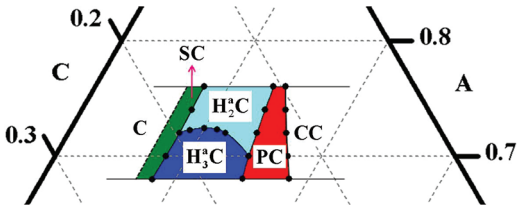

Figure 2. Portion of the supercylindrical phase region between $f_A = 0.68$ and $f_A = 0.76$ of the triangular phase diagram with given $\chi_{AB}N = \chi_{BC}N = \chi N = 80$ and $\chi_{AC} = 20$. The filled circles denote the points at which we have calculated the phase boundaries, the solid curves connecting these points are to guide the eyes, and the dashed curve without points is roughly estimated in our calculations.

region ensures that typical supercylindrical phases are obtained.[40] The second phase diagram (Figure 3) is

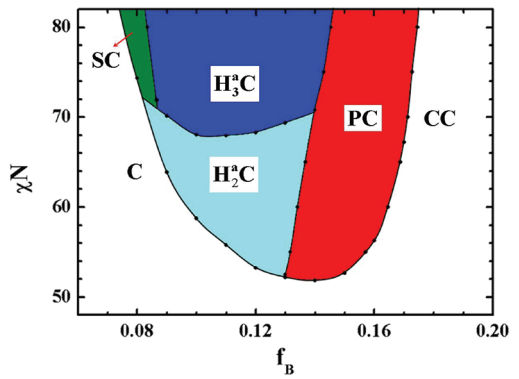

Figure 3. Portion of the phase diagram with respect to f_B and χN for fixed $\chi_{AC} = 20$ and $f_A = 0.70$.

constructed for $\chi_{AC}N = 20$ and $f_A = 0.7$ ($f_B + f_C = 0.3$), showing the dependence on the interaction parameter χN. These phase diagrams are constructed by a careful comparison

dx.doi.org/10.1021/ma2023952 | *Macromolecules* 2012, 45, 503−509

of the free energies of the candidate structures. A typical plot of the free energy difference of these phases relative to the H_2C for f_A = 0.7 is given in Figure 4. This free-energy comparison

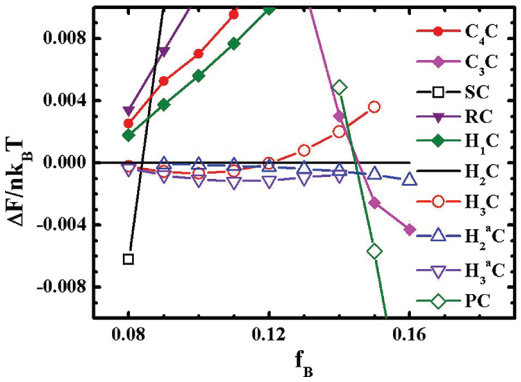

Figure 4. Free energy of various phases relative to that of H_2C, which is indicated by a solid line, as a function of f_B.

reveals that the stable phase sequence is SC, H_3^aC, PC, and CC when f_B increases (the free energy of CC is not shown for clarity). The free-energy differences between the types of double-helical and triple-helical phases are always small compared with those between the helical phases and other nonhelical ones. Both phase diagrams shown in Figures 2 and 3 suggest that only H_2^aC and H_3^aC are stable phases of the cylinders-on-cylinder type. The other two phases postulated previously by experiments or theories, C_4C and RC, are found to be metastable.

Comparing with cylinder-forming diblock copolymers under cylindrical confinement,[8,9] the B-cylinders in the current system can be considered as softly confined in the space between the concentric A and C domains. For a given set of volume fractions, both the B-cylinders and the C-cylinder have their preferred diameters because of their spontaneous curvature arising from the competition between the stretching energy and the interfacial energy. In general these preferred diameters will lead to different lengths of B- and C-cylinders. The packing of these cylinders of different lengths results in the formation of helical structures. The difference between the cylindrically confined system is that the screwing radius of the B-helices is determined by the volume fraction of the C-block in the present system, while it can be varied along with the helical pitch in the former system. For the case of straight B-cylinders, the restriction becomes stronger because the B/C-cylinders have to have equal length, and thus gives rise to a high packing frustration which results in a penalty of stretching energy. One way to release the high stretching energy is to add or remove one B-cylinder. As a consequence, the free-energy difference between two straight-cylinder phases, such as C_4C and C_3C, is rather large. For a given f_A, the change of f_B (or f_C) can significantly influence the sizes of both B-cylinders and C-cylinder, and thus influence the length ratio of the B- and C-cylinders which in turn determines the relative stability between C_4C and C_3C. When the B-cylinders are screwed onto the C-cylinder to form helices, the packing of the B-cylinders has more freedom, i.e., adjusting the pitch of helices, to reduce the packing frustration from the size mismatch. Despite this advantage, the number of helices is still a useful quantity to release the packing frustration. Similar as the transition between C_4C and C_3C, the packing of three B-helices in the reduced space becomes too crowded when the C-cylinder size is decreased, and thus, H_3^aC transfers to H_2^aC. However, the free-energy difference between the two helical phases becomes much smaller. Further analysis on this delicate transition is provided in the following content. As a special case of helices,

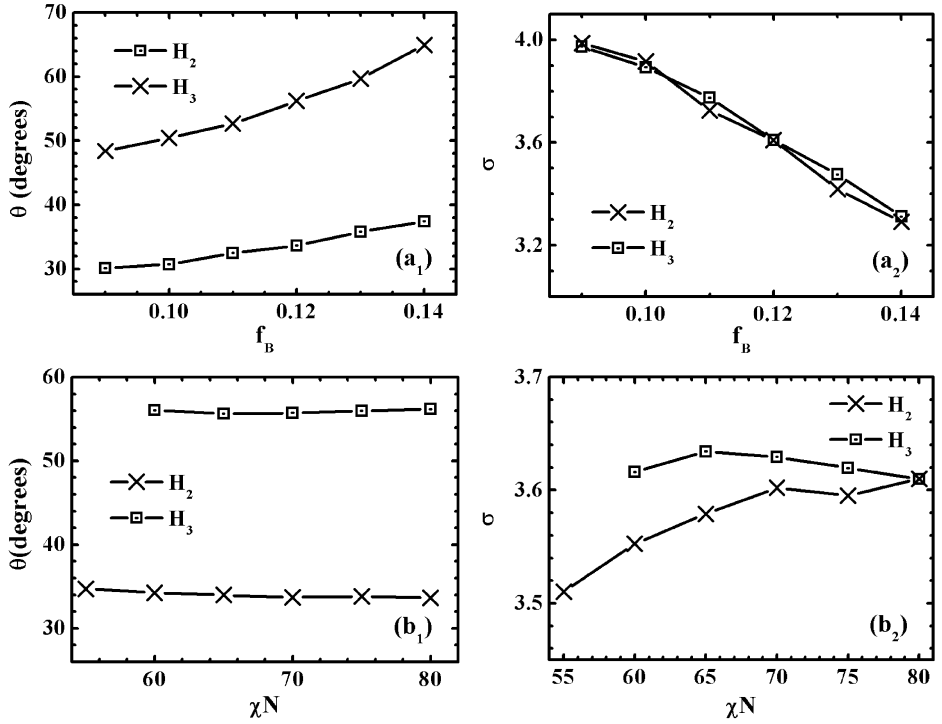

Figure 5. Pitch angle of helices and the length ratio of the B helices and the C cylinder as a function of f_B or χN for $\chi_{AC}N$ = 20. The upper row is for χN = 80 and f_A = 0.70, and the bottom row is for (f_A, f_B, f_C)= (0.70, 0.12, 0.18).

dx.doi.org/10.1021/ma2023952 | *Macromolecules* 2012, 45, 503−509

the supercylindrical phase of rings with zero pitch angle is an alternative candidate phase in which the C-cylinder can adjust its length freely to satisfy the B-cylinders. A comparison of the free-energy between RC and H_1C, reveals that RC has consistently higher free energy than the H_1C phase. This is because the bending energy of the rings in RC is higher than that of the helix in H_1C. However, the nonuniformity of chain stretching in H_1C is more pronounced compared with H_2C and H_3C, and thus it has higher free energy.

There are two notable features in the phase diagram of Figure 3. The first feature is that the B-substructure transfers from disorder (C),[41] to spheres (SC), to helices (curved cylinders), to perforated lamella (PC), and then to lamella (CC) as f_B increases. This behavior resembles the phase sequence of B/C diblock copolymers.[42] The second feature is that H_3^aC transfers to H_2^aC when χN decreases. This transition is mainly driven by the decreasing of the C-cylinder circumference which allows fewer helices to screw on it. To understand the delicate transition between H_3^aC and H_2^aC quantitatively, we calculate the length ratio between the B-cylinders (or helices) and C-cylinder, defined as $\sigma = k(1 + 1/(\tan\theta)^2)^{1/2}$, where k and θ are the number and the pitch angle of helices, respectively. The pitch angle is determined by $\theta = \tan^{-1}(L_0/2\pi r_0)$, where L_0 is the length of the supercylinder for one complete helix turn, and r_0 is the screwing radius of the helix, i.e., the distance between the maximum density point of B-helix and the center of the supercylinder. For helical phases, σ can be adjusted by varying the pitch angle to ensure that the B and C cylinders have near preferred sizes, while it is fixed as 3 or 4 for C_3C or C_4C. In Figure 5, the length ratio σ, as well as the pitch angle θ, as a function of χN or f_B, is presented. Parts a_1 and a_2 of Figure 5 are for the phase path of varying f_B for fixed parameters of $\chi N = 80$, $\chi_{AC}N = 20$, and $f_A = 0.70$ in Figure 2, and parts b_1 and b_2 are for that of varying χN for fixed compositions of (0.70, 0.12, 0.18) and interaction parameter of $\chi_{AC}N = 20$. When f_B is increased, the pitch angle of helices increases for both H_3^aC and H_2^aC, while the length ratio drops down. It is surprising that H_3^aC and H_2^aC has very close length ratios. This suggests that the two helical phases have a comparable strong capability of adjusting the sizes of both B- and C-cylinders to be close to their preferred values. This capability leads to large free-energy differences between them and those straight-cylinder phases, while small free-energy differences between themselves. When $f_B = 0.09$, the length ratio is close to 4, i.e., the length ratio of the phase C_4C. This is why the free-energy difference between C_4C and the two helical phases becomes reasonably small, but is still obviously larger than that between H_3^aC and H_2^aC. In the frustrated phases, there is a constraint arising from the architecture topology that each chain starting from the A matrix has to go through these distributed B domains, and then to enter the C domain. This means that the distribution of B domains in each phase, determining the uniformity degree of A and C chain stretching, is another factor influencing the phase stability besides the major factor of the length ratio. The phases of straight cylinders can release the chain stretching only in the plane of the cross section perpendicular to the axis of C-cylinder, while the helical phases have the third direction along the C-cylinder axis to do so. This advantage makes the helical phases have more favorable stretching energy than those of straight cylinders even when they have similar length ratio. As the length ratio drops down and deviates from 4, the free-energy difference between C_4C and the helical phases increases tremendously. Though the length ratios of the two helical phases are similar at the large value of f_B, the pitch angle of H_3^aC has been raised very large. At $f_B = 0.14$, the pitch angle is as high as 65 deg. According to this increasing tendency, we expect that the pitch angle would reach rapidly the maximum value of 90 deg for larger f_B. For the case of large pitch angles, the distribution of the B domains in H_3^aC becomes close to that of C_3C. This reason drives H_3^aC to transfer to H_2^aC which can lead to the similar length ratio but with smaller pitch angle and less constraint on the chain architecture. Besides the constraint on the chain stretching resulted by the distribution of the B-domains, the shape of the B domains can also influence the chain stretching, particularly for the B blocks. In the helical phases, the cross section perpendicular to the screwing axis is closer to an ideal shape for the B-cylinders, i.e., the preferred circle shape, for the phase with more helices (see Figure 1). The competition between the two minor factors of the distribution and the shape of the B-cylinders subtly determines the relative stability between H_3^aC and H_2^aC when they have similar length ratio. For $f_B \leq 0.14$, H_3^aC with reasonable low pitch angles is more favorable than H_2^aC. In the other case of parts b_1 and b_2, both the pitch angle and the length ratio have more moderate change as χN. Particularly the change of the pitch angle is smaller than one degree when χN varies between 55 to 80. This is because χN has similar influence on the sizes of the B- and C-cylinders. However, the B-cylinders have much larger curvature than the C-cylinder for the present asymmetric B/C composition. This fact results in increasing the size ratio of the B- and C-cylinders as χN is decreased, and thus decreasing their length ratio. Therefore, H_3^aC transfers to H_2^aC when χN is decreased.

Helices-on-cylinder have been observed in a number of experiments.[29,31−34] The compositions of the majority of these ABC triblock copolymers are located in the helical-phase regions of the current study. In particular, Jinnai et al. in a recent study have observed double-helical morphologies with antiferromagnetic arrangement of chirality by using the TEM tomography. For the composition of the PS−PB-PMMA (C: PS, B: PB, A: PMMA), i.e., (0.21, 0.09, 0.70) in their experiments, the value of χN for the stable double-helical phase is between 64 and 70 in the phase diagram of Figure 3. By taking the factor of different segment sizes into account that the PB block has relatively smaller segment size, the experimental phase point should be moved toward inside of the phase diagram.[43] In addition, a number of quantities about the superstructures and their varying tendency are comparable with our theoretical prediction. For example, the pitch and pitch angle decrease as the C block increases or the B block decreases (see Figure $5a_1$). The pitch angle, measured as 40 deg in the experiment, is different from the 30 deg estimated in our calculations. The discrepancy may be induced by the factor of the segment sizes and other uncontrollable experimental factors, such as measuring error for the pitch angle, small composition deviations, and polydispersity of polymers.

Because the helices are formed from achiral block copolymers, their chirality is not determined *a priori*. In principle we would have equal number of left-handed and right-handed helices in a given system. The arrangement of the different helices depends on the interaction between the left-handed and right-handed species. Similar to a magnetic system, the interactions can be ferromagnetic, favoring helices of the same handedness, or antiferromagnetic favoring helices of alternating handedness. Because the C-cylinders are arranged

dx.doi.org/10.1021/ma2023952 | *Macromolecules* 2012, 45, 503−509

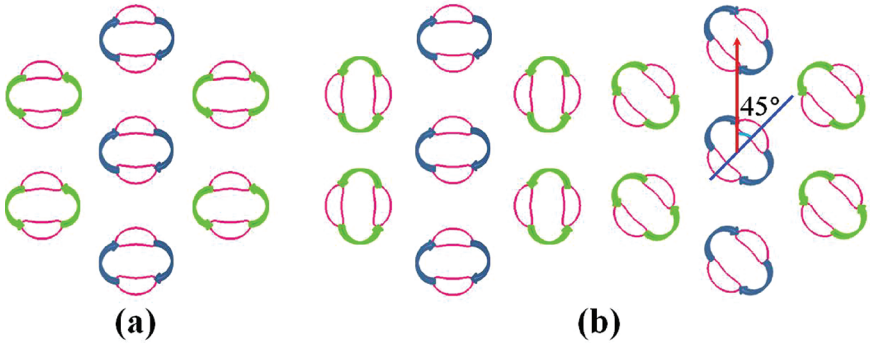

Figure 6. Schematic description of a simple arrangement of hexagonal helical supercylinders with different chiralities (indicated by various-color arrows) or rotations. (a) If the handedness is uniform, it presents as H_2C; otherwise, it presents as H_2^aC. (b) The left picture presents as $H_2^{90}C$ for uniform handedness where the helixes have a 90 deg difference of rotations between two neighbor rows; otherwise, it presents as $H_2^{a,45}$, whose cross-section with a shift of 45 deg pitch angle becomes the right picture.

on a hexagonal lattice, the state of an antiferromagnetic system is frustrated. In what follows we choose a simple arrangement for the double-helical phase illustrated in Figure 6a, i.e., the cylinders with left-handed and right-handed helices are arranged on alternative rows, which is termed as H_2^aC (the "anti" is denoted by the superscript "a"). In addition, there is a rotational freedom for each cylinder in the helical superstructures. In our calculations, we consider a number of double and triple helical phases including the two freedoms of chirality and rotation. Here we just present the free-energy comparisons of four typical double-helical phases as examples.

For a given set of parameters, $\chi_{AC}N = 20$, $\chi N = 80$, and $f_A = 0.7$, the free-energy difference, $\Delta F = F_k - F_{H_2C}$ (k indicates the other three phases, $H_2^{90}C$, $H_2^{a,45}C$, or H_2^aC), clearly shows that the antiferromagnetic H_2^aC phase among the four phases is the most favorable, and the second favorable phase, $H_2^{90}C$, has slightly higher free energy (Figure 7). The phase of $H_2^{90}C$ has

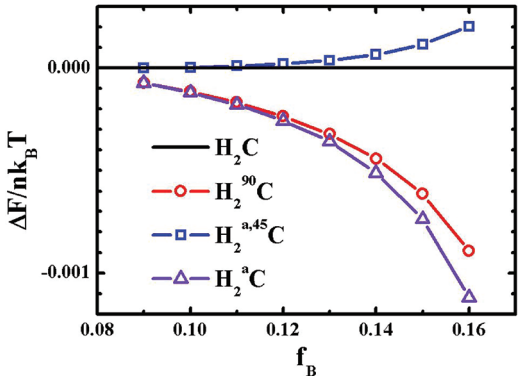

Figure 7. Free-energy of various double-helical supercylindrical phases, $H_2^{90}C$, $H_2^{a,45}C$, and H_2^aC, relative to H_2C, as a function of the volume fraction, f_B.

uniform chirality, but 90-deg rotation difference between neighbor rows of helical supercylinders. However, the free-energy difference between these phases is rather small, especially for relative small f_B. Similar to our previous results,[44] the free-energy difference between the helical phases with varying chirality and rotation is a second-order effective interaction between neighbor supercylinders, which is mainly induced by the packing of the chains.[34] This calculation provides a theoretical evidence for the observation of antiferromagnetic chiral arrangement in experiments.[32,34] Our further calculations suggest that similar conclusion can be made for the triple-helices, predicting an antiferromagnetic chiral arrangement (the H_3^aC phase).

IV. CONCLUSIONS

We have examined the formation and stability of supercylindrical phases, including quadruple/triple straight cylinders-on-cylinder, single/double/triple helices-on-cylinder, and rings-on-cylinder together with their competing phases of spheres-on-cylinder, perforated-lamella-on-cylinder, and core−shell cylinders, in frustrated ABC linear triblock copolymers. Careful comparisons of their free energy indicate that the double and triple helical phases are the stable supercylindrical phases, while the phases of single helix-on-cylinder, rings-on-cylinder, and quadruple/triple straight cylinders-on-cylinder, are metastable. The phase regions of the double/triple helical phases, surrounding by phases of spheres-on-cylinder, perforated-lamella-on-cylinder, and core−shell cylinder, are identified. Our results are well consistent with most of experimental observations of helical supercylinders, particularly with the most recent one by Jinnai et al.[34] The careful theoretical study is helpful to understand the self-assembling mechanism of these complex hierarchical phases, and is a useful guide for experiments to look for new phases, for example, the triple-helical supercylindrical phase.

The formation of the helical phases is induced by the mismatched lengths between the B- and C-cylinders because both of them have their preferred sizes for given parameters. Screwing B-cylinders around C-core-cylinder with a varying pitch angle is an efficient way to adjust the mismatched length ratio generally existing in the phases of straight cylinders. Through the analysis of the length ratio as well as the pitch angle, we find that the double and triple helical phases have similar capability on adjusting the length ratio, and thus their transition is very delicate, which has been shown by their tiny free-energy difference. Besides the major factor of the length ratio, there are two minor factors influencing the phase stability, i.e., the distribution and the shape of the B domains, which determine the uniformity degree of chain stretching. The role of the B-domain distribution arises from the constraint of the architecture topology that the polymer chain starting from A matrix has to go through B domains, and then enter C domain. When the helical phases have similar length ratio, the subtle competition between the two secondary factors determines their transition. This characteristics makes it more difficult to be

dx.doi.org/10.1021/ma2023952 | Macromolecules 2012, 45, 503−509

understood than those transitions among the helical phases in the system of cylindrically confined diblock copolymers.

In addition, we have examined the freedoms of handedness and rotation of these helical supercylinders arranged on the hexagonal lattice. By a simple arrangement of double-helical supercylinders with different chiralities, i.e., alternative rows of left-handed and right-handed helices, our calculations show that the introduction of antiferromagnetic chiralities onto neighboring helical supercylinders is preferred. In this case, the uniform rotation is most favorable, and this corresponding phase is referred as H_2^aC. In the other case of uniform chirality, $H_2^{90}C$ with a rotation difference of 90-degree on alternative rows of supercylinders is more stable than those with other values of rotation difference. However $H_2^{90}C$ consistently has slightly higher free energy than H_2^aC.

AUTHOR INFORMATION

Corresponding Author

*E-mail: weihuali@fudan.edu.cn (W.L.); fengqiu@fudan.edu.cn (F.Q.); shi@mcmaster.ca (A.-C.S.).

ACKNOWLEDGMENTS

This work is supported by the National Natural Science Foundation of China (Grants 20974026, 20990231), the National High Technology Research and Development Program of China (863 Grant No. 2008AA032101), and the Natural Science and Engineering Research Council (NSERC) of Canada. The computation was made by the facilities of SHARCNET (www.sharcnet.ca). Further computing resources were kindly provided by Dr. R. A. Wickham.

REFERENCES

(1) Chouaieb, N.; Goriely, A.; Maddocks, J. H. *Proc. Natl. Acad. Sci. U.S.A.* **2006**, *103*, 9398.
(2) Ho, R. M.; et al. *J. Am. Chem. Soc.* **2004**, *126*, 2704.
(3) Ho, R. M.; Chiang, Y. W.; Lin, S. C.; Chen, C. K. *Prog. Polym. Phys.* **2011**, *36*, 376.
(4) Ho, R. M.; et al. *J. Am. Chem. Soc.* **2009**, *131*, 18533.
(5) Wu, Y.; et al. *Nat. Mater.* **2004**, *3*, 816−822.
(6) Shin, K.; Xiang, H.; Moon, S. I.; Kim, T.; McCarthy, T. J.; Russell, T. P. *Science* **2004**, *306*, 76.
(7) Xiang, H.; Shin, K.; Kim, T.; Moon, S. I.; McCarthy, T. J.; Russell, T. P. *Macromolecules* **2005**, *38*, 1055−1056.
(8) Yu, B.; Sun, P.; Chen, P.; Jin, Q.; Ding, D.; Li, B.; Shi, A. C. *Phys. Rev. Lett.* **2006**, *96*, 138306.
(9) Li, W. H.; Wickham, R. A. *Macromolecules* **2006**, *39*, 8492.
(10) Feng, J.; Ruckenstein, E. *Macromolecules* **2006**, *39*, 4899−4906.
(11) Chen, P.; Liang, H. J.; Shi, A. C. *Macromolecules* **2007**, *40*, 7329.
(12) Sevink, G. J. A.; Zvelindovsky, A. V. *J. Chem. Phys.* **2008**, *128*, 084901.
(13) Kong, W. X.; Li, B. H.; Jin, Q. H.; Ding, D. T.; Shi, A. C. *J. Am. Chem. Soc.* **2009**, *131*, 8503.
(14) Wang, L. Q.; Lin, J. P. *Soft Matter* **2011**, *7*, 3383.
(15) Bates, F. S.; Fredrickson, G. H. *Annu. Rev. Phys. Chem.* **1990**, *41*, 525.
(16) Park, M.; Harrison, C.; Chaikin, P. M.; Register, R. A.; Adamson, D. H. *Science* **1997**, *276*, 1401.
(17) Park, C.; Yoon, J.; Thomas, E. L. *Polymer* **2003**, *44*, 6725.
(18) Bailey, T. S. *Morphological behavior spanning the symmetric AB and ABC block copolymer states*; Ph.D. Thesis, University of Minnesota, 2001.
(19) Abetz, V.; Simon, P. F. W. *Adv. Polym. Sci.* **2005**, *189*, 125.
(20) Matsen, M. W. *J. Chem. Phys.* **1998**, *108*, 785.
(21) Ranjan, A.; Morse, D. C. *Phys. Rev. E.* **2006**, *74*, 011803.
(22) Tyler, C. A.; Qin, J.; Bates, F. S.; Morse, D. C. *Macromolecules* **2007**, *40*, 4654.
(23) Guo, G.; Zhang, G.; Qiu, F.; Zhang, H.; Yang, Y.; Shi, A. C. *Phys. Rev. Lett.* **2008**, *101*, 028301.
(24) Rasmussen, K. Ø.; Kalosakas, G. J. *J. Polym. Sci., Part B: Polym. Phys.* **2002**, *40*, 1777.
(25) Tzeremes, G.; Rasmussen, K. Ø.; Lookman, T.; Saxena, A. *Phys. Rev. E.* **2002**, *65*, 041806.
(26) Fredrickson, G. H. *The Equilibrium Theory of Inhomogeneous Polymers*; Oxford University Press: Oxford, U.K., 2006.
(27) Auschra, C.; Stadler, R. *Macramolecules* **1993**, *26*, 2171.
(28) Stadler, R.; Auschra, C.; Beckmann, J.; Krappe, U.; Voigt-Martin, I.; Leibler, L. *Macromolecules* **1995**, *28*, 3080.
(29) Krappe, U.; Stadler, R.; Voigt-Martin, I. *Macromolecules* **1995**, *28*, 4558.
(30) Zheng, W.; Wang, Z. G. *Macromolecules* **1995**, *28*, 7215.
(31) Breiner, U.; Krappe, U.; Abetz, V.; Stadler, R. *Macromol. Chem. Phys.* **1997**, *198*, 1051.
(32) Elbs, H.; Abetz, V.; Hadziioannou, G.; Drummer, C.; Krausch, G. *Macromolecules* **2001**, *34*, 7917. Elbs, H.; et al. *Macromolecules* **2002**, *35*, 5570.
(33) Ludwigs, S.; Schmidt, K.; Stafford, C. M.; Amis, E. J.; Fasolka, M. J.; Karim, A.; Magerle, R.; Krausch, G. *Macromolecules* **2005**, *38*, 1850.
(34) Jinnai, H.; Kaneko, T.; Matsunaga, K.; Abetz, C.; Abetz, V. *Soft Matter* **2009**, *5*, 2042.
(35) Tang, P.; Qiu, F.; Zhang, H. D.; Yang, Y. L. *Phys. Rev. E.* **2004**, *69*, 031803.
(36) Sun, M. Z.; et al. *Phys. Rev. E.* **2008**, *77*, 016701.
(37) Shi, A.-C. *Development in Block Copolymer Science and Technology*; Hamley, I. W., Ed.; Wiley: New York, 2004).
(38) Sides, S. W.; Fredrickson, G. H. *Polymer* **2003**, *44*, 5859−5866.
(39) Frigo, M.; Johnson, S. G. FFTW: an adaptive software architecture for the FFT. *Proc. ICASSP* **1998**, *3*, 1381−1384.
(40) Abetz, V.; Goldacker, T. *Macromol. Rapid Commun.* **2000**, *21*, 16.
(41) The transition between C and CC phases is a continuous transition for varying B composition (not given in Figure 3). Even in the C phase, the B density is not uniform.
(42) Matsen, M. W.; Schick, M. *Phys. Rev. Lett.* **1994**, *72*, 2660−2663.
(43) Matsen, M. W.; Bates, F. S. *J. Polym. Sci., Part B: Polym. Phys.* **1997**, *35*, 945.
(44) Xu, Y.; et al. *J. Polym. Sci., Part B: Polym. Phys.* **2010**, *48*, 1101.